

Article

How Cracks Induced by Straining Influence the Tribological Properties of Mo Films Deposited on Polyimide Substrates

Edyta Kobierska ¹, Megan J. Cordill ^{2,*} , Robert Franz ¹ and Marisa Rebelo de Figueiredo ¹¹ Department of Materials Science, Montanuniversität Leoben, 8700 Leoben, Austria² Erich Schmid Institute of Materials Science, Austrian Academy of Sciences, Jahnstrasse 12, 8700 Leoben, Austria* Correspondence: megan.cordill@oeaw.ac.at

Abstract: Thin film materials used in flexible electronics are deposited on polymer substrates and must withstand a variety of static and dynamic mechanical loading conditions to ensure adequate reliability of the device. Tribological loads are also among these loading conditions, and suitable characterization methods and strategies are required for analyzing friction and wear for a variety of tribological contact situations. In the present work, Mo films were deposited on polyimide substrates by high-power impulse magnetron sputtering and then pre-conditioned by straining to several strain levels, including crack onset strain and strains within the crack saturation regime. Subsequently, ball-on-disk tests against different counterpart materials, namely glass, steel, and polymer, were performed to evaluate different tribological contact situations. The comparison of the results of morphologies and characteristics of the films using surface images for strained and unstrained samples provide insight into how increasing straining of the films and crack formation affect the enhanced fracture of the deposited Mo films, which served as a model system in these investigations.

Keywords: tribology; tensile straining; fragmentation; thin film; polyimide



Citation: Kobierska, E.; Cordill, M.J.; Franz, R.; de Figueiredo, M.R. How Cracks Induced by Straining Influence the Tribological Properties of Mo Films Deposited on Polyimide Substrates. *Metals* **2024**, *14*, 295. <https://doi.org/10.3390/met14030295>

Academic Editors: Ahmed Al-Kattan and Catalin Constantinescu

Received: 30 January 2024
Revised: 21 February 2024
Accepted: 28 February 2024
Published: 1 March 2024



Copyright: © 2024 by the authors. Licensee MDPI, Basel, Switzerland. This article is an open access article distributed under the terms and conditions of the Creative Commons Attribution (CC BY) license (<https://creativecommons.org/licenses/by/4.0/>).

1. Introduction

The development of stretchable, biocompatible materials, as well as low-cost and advanced manufacturing technology, fuel the advances of flexible electronics. Today, foldable displays are already commercially available in portable phones, laptops, and other electronic products [1], while flexible photovoltaics can be added to complex surfaces or integrated with other devices to enable self-powered electronics [2]. Furthermore, high-precision medical devices and wearable sensors for monitoring various physiological signals for the assessment of human health and remote diagnosis are in development [3,4]. Additionally, in industries such as automotive engineering and aerospace, the demand for flexible and lightweight materials is growing rapidly. For example, the automotive industry requires flexible materials for the fabrication of next-generation vehicles with improved fuel efficiency and crash safety [5], while aerospace engineers need flexible structures for aircraft components, such as wings and fuselage [6]. In aircraft, tribological studies help optimize the performance of bearings to withstand demanding conditions while minimizing maintenance requirements and downtime. Materials used for such applications have to maintain consistent electrical and mechanical properties under a variety of loading conditions, where systems combining rigid films on compliant polymer substrates are one of the material systems important for flexible device design [7].

Rigid substrates behave differently compared to flexible ones, and understanding these distinctions is vital for optimizing the mechanical reliability of thin-film polymer systems, especially in the context of tribology. In rigid systems, the substrate provides rigid support, leading to more uniform stress distribution and a reduced likelihood of deformation [8–10]. On the other hand, flexible substrates offer greater conformability and

can withstand bending and stretching without failure, making them ideal for applications requiring flexibility and durability, such as tribological settings [11,12]. Understanding these differences is crucial for designing thin-film polymer systems tailored to specific applications, as mechanical properties must be carefully balanced to ensure optimal performance and reliability.

To investigate the tensile strength of thin films, a considerable number of techniques have been developed and used, such as scratch testing, peel testing, or cyclic testing in bending or stretching modes. Among them, the fragmentation test, which can examine the gradual failure of the brittle films under uniaxial tension as a function of substrate strain or stress, has been found to be suitable for a wide range of material combinations [13]. It provides a direct and accurate assessment of the film's internal stress state and excludes third body interactions that are present in other methods. There are several works in the literature dealing with fragmentation observed in uniaxial loading, from theoretical analyses [14,15] to simulations of fragmentation formation [16,17] and observations of cracking phenomena [18].

As thin films on polymer material systems are used in demanding technological applications, such as flexible electronics, tailored mechanical and chemical properties have to be achieved [19,20]. Testing the mechanical reliability of thin-film polymer systems is essential for the optimization of material design and processing techniques to achieve tailored mechanical properties and ensure the long-term reliability of such systems. By subjecting these materials to cyclic loading, fatigue testing simulates real-world conditions and helps identify potential failure modes such as (interfacial) crack propagation and delamination over time [21,22]. These failure mechanisms pose significant challenges to the reliability of thin films, particularly in applications subjected to dynamic or cyclic loading, such as flexible electronics [23,24]. Tribology also becomes increasingly important for such technological applications. In the specific case of thin films on polymers used in flexible electronics, film damage due to friction and wear are undesirable. However, little work has been done in this respect, in particular combining straining and tribological exposure of the films. The latter is of critical importance, as failure mechanisms may originate from the interplay between the strain applied to a thin film supported by a polymer system and friction and wear when in sliding contact with a counterpart material. The aim of this study is to investigate tribological properties of a model system of molybdenum thin film on polyimide (PI) that reproducibly cracks under uniaxial straining, with focus on the appearance of the wear scars after tribological tests with different counterparts.

2. Materials and Methods

Mo thin films were grown on PI foil type UPILEX-S by high-power impulse magnetron sputtering (HiPIMS). Before deposition, PI substrates with a thickness of 125 μm were cut into crosses and strips, cleaned in ultrasonic baths of ethanol, and blow-dried. Afterwards, they were positioned onto a substrate holder and placed into a deposition chamber, which was then evacuated to a base pressure below 1×10^{-6} Pa. Mo films with a nominal thickness of 1 μm were grown during a 30 min deposition, using a Mo target with a diameter of 76 mm at an Ar flow of 8 sccm, which corresponds to a pressure of 0.5 Pa. The HiPIMS pulses used had a repetition frequency of 100 Hz and a pulse-on time of 200 μs . No substrate bias or external heating was applied during deposition.

Uniaxial tensile straining was performed on cross-shaped samples with an approximate length of 5 cm and an arm width of 0.5 cm. A cross-shaped sample was necessary to have a large enough area for the tribological tests. The samples were strained using a custom-built screw-driven small-scale straining stage designed specifically to perform under a three-dimensional (3D) confocal laser scanning microscope (CLSM, Keyence, Mechelen, Belgium) [25]. The CLSM was used to record the Mo surface and to observe the amount of mechanical damage, or cracks, during straining. As the custom-built stage can only be used in displacement control, the strain was calculated using the distance between the grips at various displacement steps. At each straining step, an image of the same area

was measured. The crack spacing, λ , was then evaluated by counting the number of cracks intersecting the line across an entire image of a surface area size of $97 \mu\text{m} \times 73 \mu\text{m}$. Three lines were used for every image, and the average crack density was calculated as the ratio between the average number of cracks visible and the length of the image.

In order to capture the electrical behavior, additional uniaxial tensile tests were performed with an MTS Tytron 250[®] universal testing machine, while recording the change in electrical resistance with a four-point probe configuration [26]. Three strip samples ($6 \text{ mm} \times 35 \text{ mm}$) were strained continuously to a maximum elongation of 12% with an initial gauge length of 20 mm and a displacement rate of $5 \mu\text{m/s}$. The tensile critical failure strain was defined by the crack onset strain (COS) as the strain at which the measured resistance increased by 10% compared to the resistance of the unloaded sample. Such a convention was introduced to allow for a comparison of data from various research groups [27].

The tribological behavior was evaluated at room temperature on a ball-on-disk tribometer (CSM Instruments, Filderstadt, Germany) with the same set-up as in [28]. Coated polymer samples were attached to a glass plate, which had a thickness of around 10 mm. This was carried out to offer support and enable the specimen to be secured in the experimental configuration because the device was originally designed for testing rigid discs. It is important to note that the samples underwent fatigue loading exclusively and were cyclically loaded through the sample disc rotating under the stationary loaded ball counterpart. The complete modified experimental set-up is detailed in the preceding publication [28]. The counterpart balls with a diameter of 6 mm were made of soda lime glass (SLG), a 100Cr6 ball-bearing steel, and polyether ether ketone (PEEK). Tribological tests were performed for 1000 laps, applying a normal load, radius, and linear speed of 0.626 N, 2 mm, and 0.5 cm/s, respectively. To ensure the reliability of our findings, each strain condition and counterpart combination underwent three tribological tests where a new sample was used each time. The surface appearance of the Mo film and the counterpart balls after tribological testing was evaluated using the same CLSM as mentioned above. The general shape of the scar was circular or oval with groves in the middle that were parallel to the direction of sliding. Due to the stress in the Mo film induced by the deposition using HiPIMS, a slight curvature of the PI substrate was present, causing a slight oscillation of the counterpart motion in the z-direction (vertical to the wear track) during one lap. This may be the reason for the slightly non-circular shapes of the counterpart wear scars. It should be noted that after removal of the samples from the straining device and prior to performing the tribological tests, the cracks closed as the sample relaxed, and the cracks were not visible via investigations using a CLSM. Similar behavior of crack closure has been reported for ductile Cu films on polymer substrates [29]. However, the cracks could be evidenced inside the wear track after the tribological tests regardless of the counterpart material used due to the additionally induced strain on the film in the tribological contact zone and wear effects.

3. Results and Discussion

The synthesized Mo films resulted in a nominal thickness of $1 \mu\text{m}$ and a surface roughness of $26 \pm 2 \text{ nm}$. It was observed that after straining up to 5%, the surface roughness increased to $37 \pm 4 \text{ nm}$, suggesting alterations in the film morphology induced by mechanical deformation. Previous investigations of these film and substrate systems [28] also encompassed X-ray diffraction (XRD) measurements, which exclusively revealed Mo peaks, indicating the purity of the films.

The Mo film's electrical response to uniaxial tensile stress is shown in Figure 1. The normalized resistance R/R_0 is shown as a function of engineering strain, where R_0 stands for the initial resistance, and R represents the instantaneous measured resistance. During loading, R/R_0 increases continuously following the theoretical constant volume approximation (theory in Figure 1) [30] when the film remains undamaged and electrically conductive. After exceeding the critical failure strain characterized by the COS at $1.7\% \pm 0.2\%$, the resis-

tance experiences a sharp increase. The COS value was determined using a 10% deviation from the constant volume approximation. The sharp increase in the electrical resistance is indicative of brittle films on polymer substrates [27].

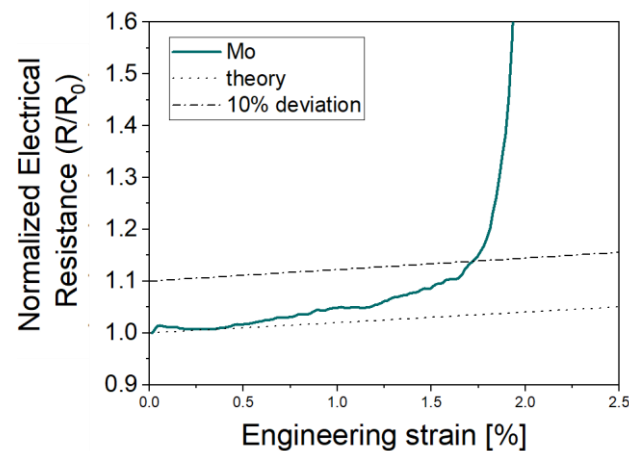


Figure 1. Representative change in electrical resistance as a function of the applied strain for the Mo film. Dotted and dashed lines depict the constant volume approximation (theory) and a 10% deviation; R is the resistance, and R_0 is the initial resistance.

A brittle film can start to fracture under tensile straining at low applied strains, and with more strain, cracks continue to develop until the saturation crack spacing is attained, and cracks can no longer develop between already existing fragments [31,32]. Afterwards, the film may buckle and delaminate as a result [33]. The evolution of cracks developed in the Mo film with increasing applied uniaxial strain from 1% to 6% is shown in Figure 2. Short parallel cracks start appearing in the film after 1% strain, and the density of cracks increases with increasing applied strain. Between 5% and 6%, no new cracks emerge between already existing cracks, which indicates that the saturation regime was achieved. Based on the obtained result regarding the COS and observed progression in crack spacing, two strains were selected for the preconditioning of the tribological samples, namely, 2% and 5%, in addition to the as-deposited condition (0%). The value of the 2% strain was just above the COS, resulting in large crack spacing in the Mo film, while at a strain of 5%, the crack saturation regime was reached (smaller crack spacing). The average saturation crack spacing of $38.8 \pm 12.8 \mu\text{m}$ was measured from the recorded CLSM images of the surface after 6% applied strain.

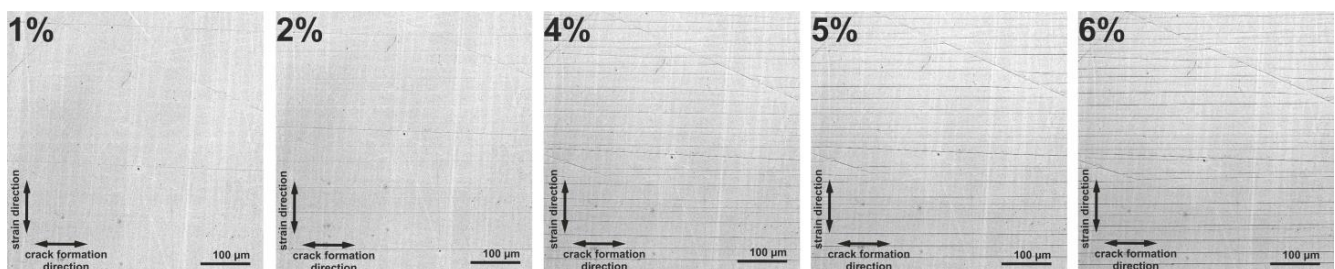


Figure 2. Crack evolution on the surface of the Mo film strained up to 6%. All images are taken under load to enhance the visibility of the cracks. The straining direction is in a vertical direction.

During the ball-on-disc tests against the three counterparts, all the samples, regardless of the strain level, revealed similar values for the coefficient of friction (COF), with the majority of the COF values falling between 0.5 and 1.5, which is in agreement with a previous work [28]. Cracks that appeared on the film surface with straining were without significant effect on the friction. An overview of the surface morphologies of the Mo film on PI after tribological testing against the SLG counterpart is shown in Figure 3. Deep grooves

going through the entire film to the substrate can be observed in all the cases, indicative of abrasive wear mechanisms characterized by material removal through ploughing and cutting actions [34]. Another distinctive feature in all the samples is the secondary crack pattern in the wear track, which is an indication of fatigue due to repeated loading and unloading of the film as the counterpart passes [34]. Loose material of broken film can be seen mostly on the outside of the wear track as wear debris, further emphasizing abrasive wear. In the images of the samples exposed to straining to 2% and 5%, there are visible lines going across the width of the wear track, portraying cracks in the film that resulted from the pre-conditioning (straining) procedure. Increased strain caused an increased number of cracks to be visible on the surface. The secondary cracks are similar to biaxially induced cracks [35] and have smaller spacing compared to the cracks induced via straining.

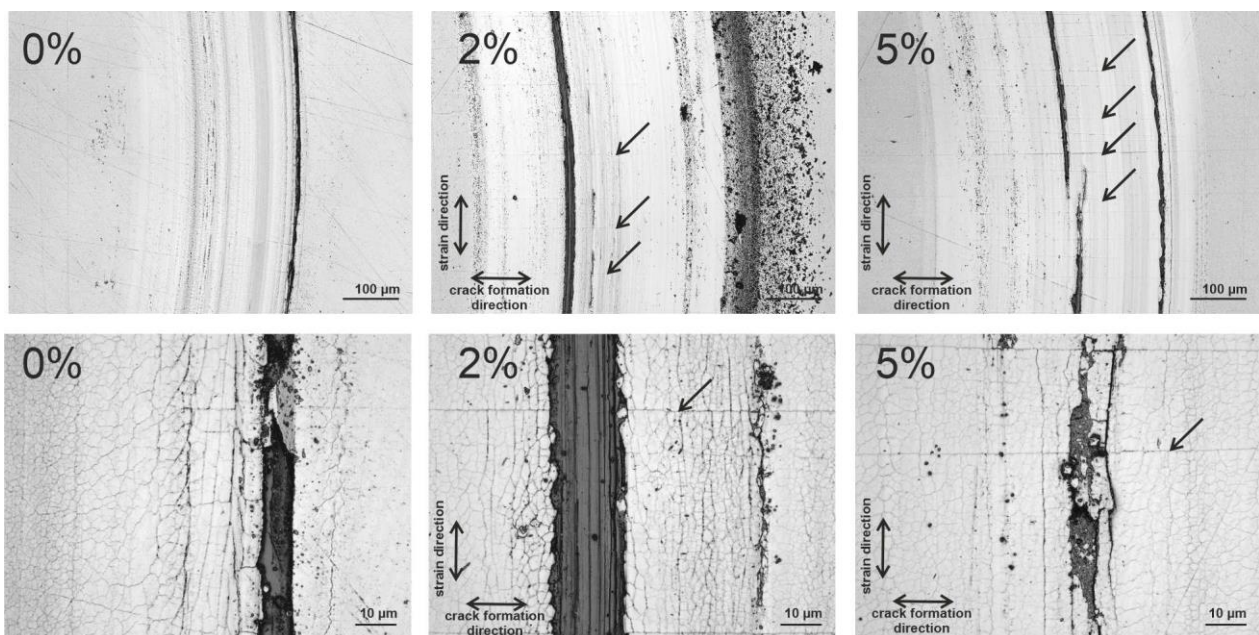


Figure 3. Laser intensity images of wear tracks on Mo films after straining to 0%, 2%, and 5% and ball-on-disk tests against SLG. The first row illustrates the general view of the produced wear tracks. The second row shows images with higher magnification and the secondary cracking that occurred during tribological loading. The arrows in all the images mark the position of cracks induced by straining.

No pronounced influence of the cracks was observed in regions where the cracks were perpendicular to the sliding direction, as shown in Figure 3. However, in places with an oblique angle between cracks and sliding direction, additional effects were observed, as illustrated in Figure 4, for the sample that was strained to 2% strain prior to the tribological test. Mo film fragments in these places broke off directly in a line going from the horizontal crack to the already existing groove in the wear track, creating triangular shaped wear features (see marked areas in Figure 4). In addition to enhanced film material removal at the crack lines, wear debris was redistributed within the wear track and accumulated at open crack edges (see marked area in Figure 4). This material remains within the wear track and does not contribute to the wear debris outside the wear track at this stage of the wear test. Again, secondary cracks are also visible and follow the circular path of the counterpart. The cracks that form due to pre-conditioning act as concentration points for film fragments to be removed or as collection points for the generated debris.

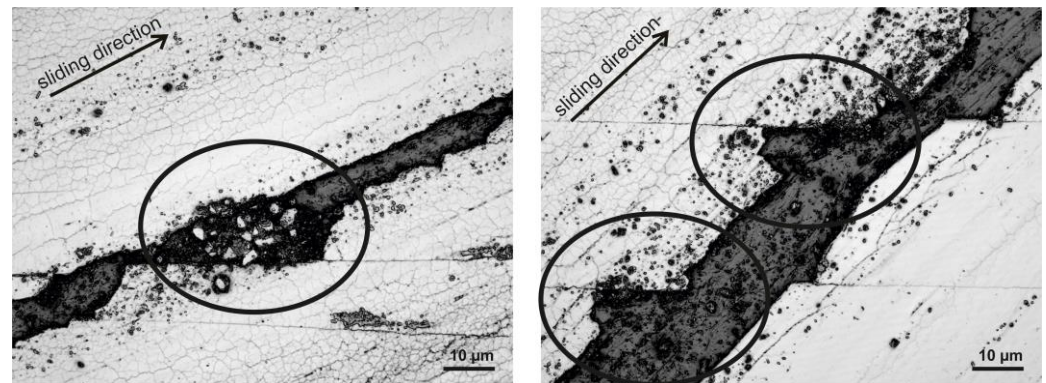


Figure 4. Laser intensity images of wear tracks after ball-on-disk tests against the SLG counterpart on Mo films strained to 2% to illustrate that, at oblique angles to the strain-induced cracks, wear debris is collected (**left image**) or more removed (**right image**), perpendicular to the cracks. The arrows in the top left of the images indicate the sliding direction of the counterpart.

By increasing the strain from 2% to 5%, the number of cracks increases, and, hence, the number of sites with additional film removal and accumulation also increases, as shown in Figure 5. Film fragment removal can lead to a widening of the wear track compared to the areas where the counterpart path is more perpendicular to the cracks (see Figure 3) and an enhanced wear in such regions as triangular-shaped wear features are joined and enlarged. In the present case, the wear track width, defined here as the width of the track where PI is visible (very dark or black areas in the figures) increased from 5 to 10 µm for the 0% and 2% strained samples up to values of 80 µm for the samples preconditioned with 5% applied strain.

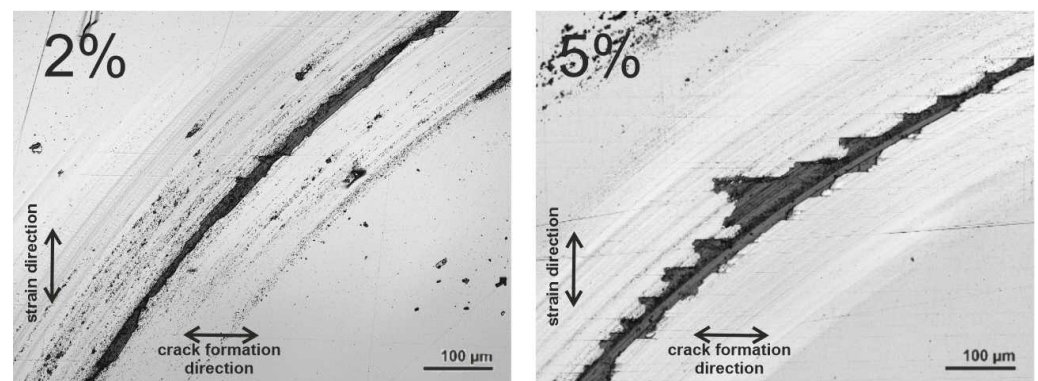


Figure 5. Laser intensity images of wear tracks with exposed substrate after ball-on-disk tests against SLG counterpart on Mo films strained to 2% and 5%. Comparing the 2% strained with the 5% strained sample, with a smaller crack spacing (higher crack density), more of the Mo film is removed.

The results of the tribological tests against the steel counterpart, 100Cr6, are illustrated in Figure 6 and reveal similar wear behavior. As was the case for SLG, grooves down to the substrate are formed in the wear track alongside secondary fatigue crack pattern with fragmentation and film removal in the tribological contact zone. This generally similar behavior can be understood by the comparable hardness of the 100Cr6 counterpart to the SLG counterpart. The influence of the cracks from straining is slightly different, as larger Mo film fragments were removed in the vicinity of cracks in the case of the 100Cr6 counterpart as compared to the SLG counterpart. Such fragments can have a size of about 20 µm compared to size of 8 ± 2 µm for SLG. Figure 7 shows removed fragments in a sample tested against 100Cr6 that was strained to 5%. The fragment size is around the same size as the saturation crack spacing. The interaction between the relatively hard counterparts and the Mo film contribute to material loss and surface degradation over time.

These observations collectively highlight the predominance of abrasive wear mechanisms in the tribological behavior of the SLG and 100Cr6 counterpart on Mo film.

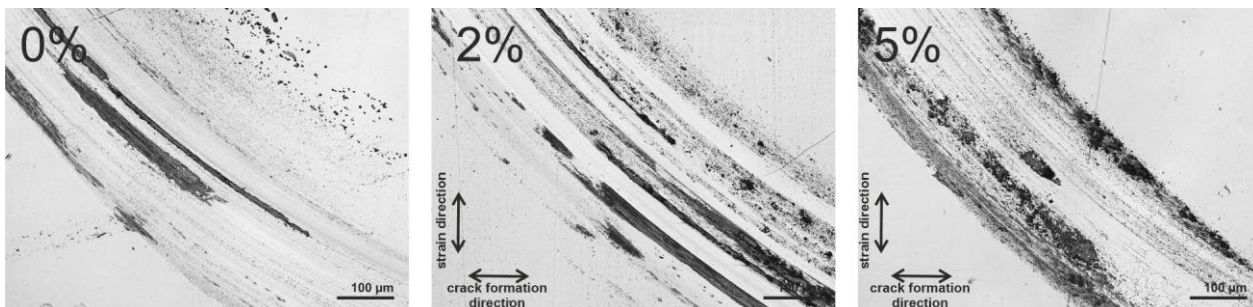


Figure 6. Laser intensity images of wear tracks on Mo films after straining to 0%, 2%, and 5% and ball-on-disk tests against the 100Cr6 counterpart.

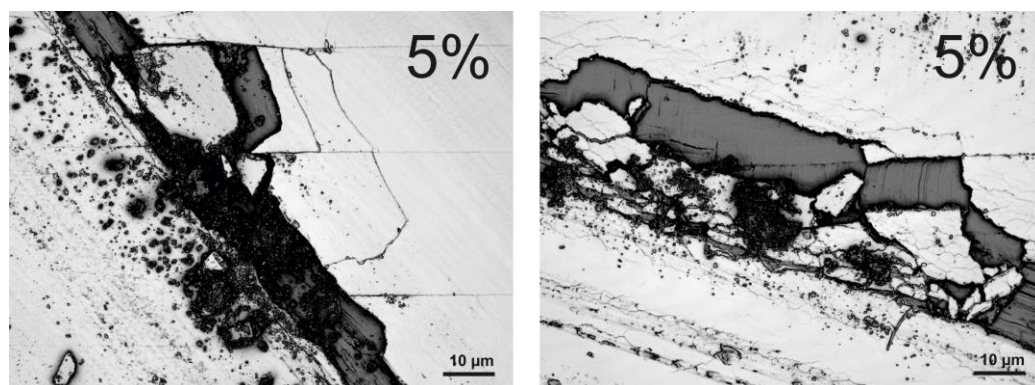


Figure 7. Laser intensity image of cracks with an oblique angle to the wear tracks from ball-on-disk tests against the 100Cr6 counterpart on Mo films strained to 5%. A secondary cracking pattern is observed as well as film fragment removal and accumulation in areas more oblique to the strain-induced cracks.

A different situation was encountered when using PEEK as the counterpart in the tribological tests. The surface of the films after testing was largely unchanged, and no pronounced wear track was observed, as shown in Figure 8. Due to the low hardness of PEEK, the wear behavior differed significantly from that observed with SLG and 100Cr6. Instead of deep grooves and fragmentation, the Mo film surface was mainly polished, and only a few shallow grooves were observed. The wear mechanism observed when using PEEK as the counterpart in the tribological tests can be described as primarily abrasive wear, coupled with some degree of polishing. Additionally, the presence of cracks was without significant influence on the wear behavior. Most notably was that film fragment removal from crack edges and the secondary fatigue crack patterns as observed for SLG and 100Cr6 were absent in the case of the PEEK counterpart, highlighting a distinct wear mechanism characterized by polishing and minimal material removal.

The wear scars on the counterparts, as shown in Figure 9, have a different appearance, depending on the mechanical properties and the surface structure of the counterpart, as well as the behavior when in contact with the Mo film. The SLG counterpart had small depressions on the outside in its original state, which are still partly visible in the wear scar of the counterpart after the tribological test. In this instance, film fragments accumulated at the back of the worn area on the counterparts. Straining the Mo film influenced the amount of the accumulated material on the counterparts but did not appear to be significant. The surface of the 100Cr6 counterpart did not have the distinguishing features of all three counterparts initially, and the wear scar can easily be observed. In this case, the groves left from sliding were shallower and, in contrast to SLG, the Mo film fragments accumulated

not only at the back of the wear scar but also in the center region. The straining of the Mo film had a similar effect, indicating that an increase in wear debris material was noticeable with increase in straining. Finally, the PEEK counterparts had the most structured surface, with the deepest impressions of all three counterpart materials. Furthermore, the wear scars are least pronounced in the case of the PEEK counterparts. This can be understood by the fact that the PEEK counterpart material had the lowest hardness, and film fragments were not removed during the tribological test, and only smooth wear tracks were observed on the Mo film as well as on the PEEK counterpart. As only very little wear debris was generated in the tests against PEEK, no particles accumulated at the front of the wear scar of the ball. This observation is independent of the prior straining of the Mo film.

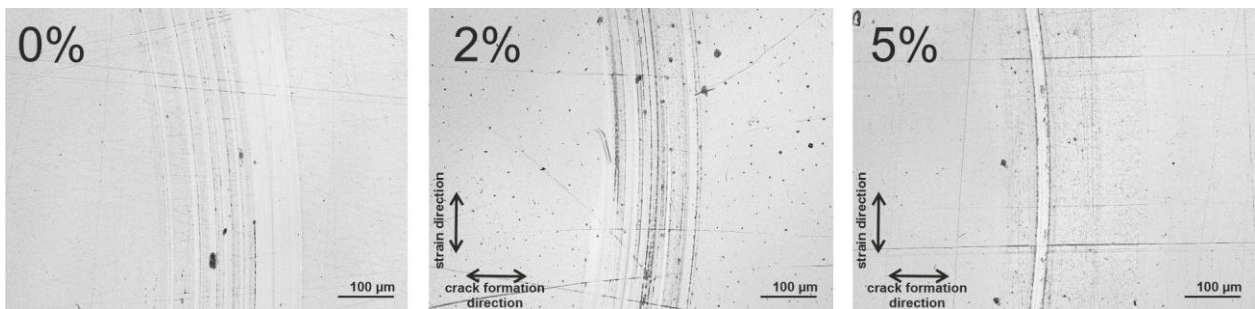


Figure 8. Laser intensity images of wear tracks on Mo films after staining to 0%, 2%, and 5% and ball-on-disk tests against the PEEK counterpart. Neither the secondary crack pattern nor film removal was observed for these samples.

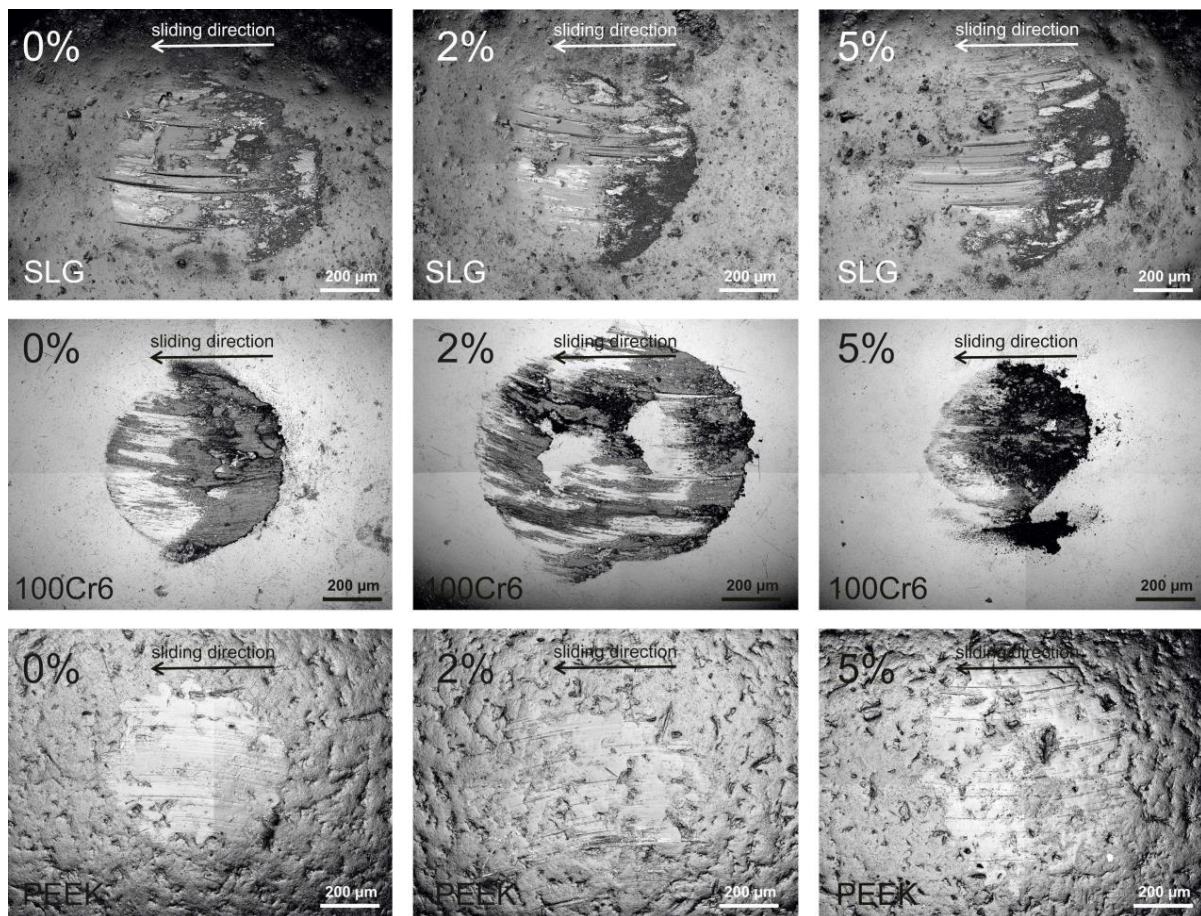


Figure 9. Laser intensity images of the wear scars on the ball counterparts after ball-on-disk tests.

4. Conclusions

The effect of straining on the wear behavior of Mo films deposited by HiPIMS onto compliant polymer foils was investigated. The characterization of the cracks induced by applying uniaxial tensile strain revealed that a crack saturation regime was reached at around 5% applied engineering strain. When the Mo films were tested against 100Cr6 and SLG counterparts, a combination of fatigue and abrasive wear—the latter caused by the ploughing of transfer material—was observed, and wear debris accumulated outside and inside the circular wear track. In areas where the cracks were perpendicular to the sliding direction, no significant impact of the cracks on wear behavior was seen. By contrast, enhanced fracture and more film fragment removal were observed, where an oblique angle between the cracks and sliding direction was present. Minimal changes in wear tracks were observed when testing against the soft PEEK counterpart after straining, with limited material transfer. Overall, the results show that the proposed approach of using ball on-disc tests on strained metallic films and compliant substrates is a suitable technique to gain insight about the effect of induced cracks on tribological behavior, especially as the angle between the cracks and the sliding direction is a major factor of influence. Moving forward, further exploration into the interplay between crack morphology and wear mechanisms will be crucial for advancing our understanding of tribological phenomena in heterogeneous material systems.

Future research in this field could explore several avenues to deepen our understanding of tribological behavior in thin-film and compliant substrate systems. Intermittent characterization techniques during tribological testing, such as scanning electron microscopy (SEM) or atomic force microscopy (AFM), could offer visualization of the evolving wear processes and help elucidate the underlying mechanisms at a finer scale. Moreover, studying the long-term stability and reliability of these systems under cyclic loading and extended tribological exposure could provide valuable insights into their sustainability for practical applications in various fields, such as flexible electronics, biomedical devices, and aerospace components. Future research endeavors aimed at addressing these challenges could significantly advance the current understanding of tribological phenomena in thin-film and compliant substrate systems and pave the way for the development of more robust and reliable materials and devices.

Author Contributions: Conceptualization, E.K., R.F. and M.R.d.F.; methodology, E.K. and M.R.d.F.; formal analysis, E.K., R.F. and M.R.d.F.; writing—original draft preparation, E.K., M.J.C., R.F. and M.R.d.F.; writing—review and editing, M.J.C.; visualization, E.K.; supervision, M.J.C., R.F. and M.R.d.F.; funding acquisition, M.R.d.F. All authors have read and agreed to the published version of the manuscript.

Funding: This research was funded by the Austrian Science Fund, FWF, under project number P 32289-N37.

Data Availability Statement: The raw data supporting the conclusions of this article will be made available by the authors on request.

Acknowledgments: P. Kreiml is acknowledged for experimental assistance.

Conflicts of Interest: The authors declare no conflicts of interests. The funders had no role in the design of the study, in the collection, analysis, interpretation of the data, writing of the manuscript or in the decision to publish the results.

References

1. Lee, J.C.; Hudson, S.E.; Tse, E. Foldable Interactive Displays. In Proceedings of the UIST, Association for Computing Machinery, Monterey, CA, USA, 19–22 October 2008; pp. 287–290.
2. Dong, P.; Rodrigues, M.T.F.; Zhang, J.; Borges, R.S.; Kalaga, K.; Reddy, A.L.M.; Silva, G.G.; Ajayan, P.M.; Lou, J. A Flexible Solar Cell/Supercapacitor Integrated Energy Device. *Nano Energy* **2017**, *42*, 181–186. [[CrossRef](#)]
3. Zhou, J.; Men, D.; Zhang, X.E. Progress in Wearable Sweat Sensors and Their Applications. *Chin. J. Anal. Chem.* **2022**, *50*, 87–96. [[CrossRef](#)]

4. Zhou, C.; Shi, N.; Jiang, X.; Chen, M.; Jiang, J.; Zheng, Y.; Wu, W.; Cui, D.; Haick, H.; Tang, N. Techniques for Wearable Gas Sensors Fabrication. *Sens. Actuators B Chem.* **2022**, *353*, 131133. [[CrossRef](#)]
5. Patil, A.; Patel, A.; Purohit, R. An Overview of Polymeric Materials for Automotive Applications. *Mater. Today Proc.* **2017**, *4*, 3807–3815. [[CrossRef](#)]
6. Ghori, S.W.; Siakeng, R.; Rasheed, M.; Saba, N.; Jawaid, M. *The Role of Advanced Polymer Materials in Aerospace*; Elsevier Ltd.: Amsterdam, The Netherlands, 2018; ISBN 9780081021316.
7. Ansari, M.S.; Othman, M.H.D.; Ansari, M.O.; Ansari, S.; Abdullah, H.; Harun, Z. Magnetite Thin Films Grown on Different Flexible Polymer Substrates at Room Temperature: Role of Antiphase Boundaries in Electrical and Magnetic Properties. *J. Alloy Compd.* **2020**, *846*, 156368. [[CrossRef](#)]
8. Salhi, F.; Aissani, L.; Fellah, M.; Chadli, A.; Cheriet, A.; Belgroune, A.; Nouveau, C.; Obrosof, A.; Abdul Samad, M.; Alhussein, A. Experimental Investigation of Structural, Wetting, Mechanical and Tribological Properties of TiZrN Thin Films Deposited by Magnetron Sputtering. *Surf. Interfaces* **2021**, *27*, 101519. [[CrossRef](#)]
9. Vuchkov, T.; Evaristo, M.; Yaqub, T.B.; Cavaleiro, A. The Effect of Substrate Location on the Composition, Microstructure and Mechano-Tribological Properties of W-S-C Coatings Deposited by Magnetron Sputtering. *Surf. Coat. Technol.* **2020**, *386*, 125481. [[CrossRef](#)]
10. Aissani, L.; Alhussein, A.; Ayad, A.; Nouveau, C.; Zgheib, E.; Belgroune, A.; Zaabat, M.; Barille, R. Relationship between Structure, Surface Topography and Tribo-Mechanical Behavior of Ti-N Thin Films Elaborated at Different N₂ Flow Rates. *Thin Solid Film.* **2021**, *724*, 138598. [[CrossRef](#)]
11. Xu, Y.; Jia, J.; Zhang, G.; Li, H.; Chen, T. Effect of Rubber Substrates on the Flexibility and Tribological Properties of Diamond-like Carbon Coatings. *Surf. Coat. Technol.* **2021**, *422*, 127526. [[CrossRef](#)]
12. Wu, Y.; Wang, Y.; Li, Y. Combining the Good Tribological Properties with the High Adhesion Strength of the Amorphous Carbon Films in Situ Grown on PI. *Front. Mater.* **2023**, *10*, 1138854. [[CrossRef](#)]
13. Tavares da Costa, M.V.; Bolinsson, J.; Neagu, R.C.; Fayet, P.; Gamstedt, E.K. Experimental Assessment of Micromechanical Models for Fragmentation Analysis of Thin Metal Oxide Coatings on Polymer Films under Uniaxial Tensile Deformation. *Surf. Coat. Technol.* **2019**, *370*, 374–383. [[CrossRef](#)]
14. Andersons, J.; Tarasovs, S.; Leterrier, Y. Analysis of Thin Film Cracking and Buckling on Compliant Substrate by Fragmentation Test. *Key Eng. Mater.* **2007**, *348–349*, 329–332. [[CrossRef](#)]
15. Leterrier, Y.; Wyser, Y.; Manson, J.A.E.; Hilborn, J. A Method to Measure the Adhesion of Thin Glass Coatings on Polymer Films. *J. Adhes.* **1994**, *44*, 213–227. [[CrossRef](#)]
16. Yu, Y.; Tang, W.; Liu, Z.; Bai, L. Deformation Mechanisms of Si-Doped Diamond-like Carbon Films under Uniaxial Tension Conditions. *Diam. Relat. Mater.* **2020**, *110*, 108099. [[CrossRef](#)]
17. He, Y.; Li, H.; Wei, F.; Qi, J.; Meng, Q.; Sui, Y. Mechanical Properties of Multilayer Hexagonal Silicon under Uniaxial Tension. *Comput. Mater. Sci.* **2017**, *134*, 153–159. [[CrossRef](#)]
18. Jansson, N.E.; Leterrier, Y.; Manson, J.A.E. Modeling of Multiple Cracking and Decohesion of a Thin Film on a Polymer Substrate. *Eng. Fract. Mech.* **2006**, *73*, 2614–2626. [[CrossRef](#)]
19. Choi, M.C.; Kim, Y.; Ha, C.S. Polymers for Flexible Displays: From Material Selection to Device Applications. *Prog. Polym. Sci.* **2008**, *33*, 581–630. [[CrossRef](#)]
20. Lee, J.A.; Lin, C.R.; Pan, P.C.; Liu, C.W.; Sun, A.Y.T. Dramatically Enhanced Mechanical Properties of Diamond-like Carbon Films on Polymer Substrate for Flexible Display Devices via Argon Plasma Pretreatment. *Chem. Phys.* **2020**, *529*, 110551. [[CrossRef](#)]
21. Shen, Y.; Feng, Z.; Zhang, H. Study of Indium Tin Oxide Films Deposited on Colorless Polyimide Film by Magnetron Sputtering. *Mater. Des.* **2020**, *193*, 108809. [[CrossRef](#)]
22. Brenneman, J.; Tansel, D.Z.; Fedder, G.K.; Panat, R. Interfacial Delamination and Delamination Mechanism Maps for 3D Printed Flexible Electrical Interconnects. *Extrem. Mech. Lett.* **2021**, *43*, 101199. [[CrossRef](#)]
23. Badrudin, S.I.; Noor, M.M.; Abd Samad, M.I.; Zakaria, N.S.N.; Yunas, J.; Latif, R. Eliminating Surface Cracks in Metal Film-Polymer Substrate for Reliable Flexible Piezoelectric Devices. *Eng. Sci. Technol. Int. J.* **2024**, *50*, 101617. [[CrossRef](#)]
24. Li, J.; Fang, L.; Sun, B.; Li, X.; Kang, S.H. Review—Recent Progress in Flexible and Stretchable Piezoresistive Sensors and Their Applications. *J. Electrochem. Soc.* **2020**, *167*, 037561. [[CrossRef](#)]
25. Cordill, M.J.; Marx, V.M. Fragmentation Testing for Ductile Thin Films on Polymer Substrates. *Philos. Mag. Lett.* **2013**, *93*, 618–624. [[CrossRef](#)]
26. Glushko, O.; Cordill, M.J. Electrical Resistance of Metal Films on Polymer Substrates under Tension. *Exp. Tech.* **2016**, *40*, 303–310. [[CrossRef](#)]
27. Cordill, M.J.; Kreiml, P.; Mitterer, C. Materials Engineering for Flexible Metallic Thin Film Applications. *Materials* **2022**, *15*, 926. [[CrossRef](#)]
28. Kobierska, E.; Zak, S.; Hirn, S.; Cordill, M.J.; Franz, R.; de Figueiredo, M.R. Tribological Investigations of Mo Films Deposited on Thin Polyimide Substrates. *Surf. Coat. Technol.* **2022**, *442*, 128549. [[CrossRef](#)]
29. Glushko, O.; Marx, V.M.; Kirchlechner, C.; Zizak, I.; Cordill, M.J. Recovery of Electrical Resistance in Copper Films on Polyethylene Terephthalate Subjected to a Tensile Strain. *Thin Solid Film.* **2014**, *552*, 141–145. [[CrossRef](#)]
30. Xiang, Y.; Li, T.; Suo, Z.; Vlassak, J.J. High Ductility of a Metal Film Adherent on a Polymer Substrate. *Appl. Phys. Lett.* **2005**, *87*, 161910. [[CrossRef](#)]

31. Agrawal, D.C.; Raj, R. Measurement of the Ultimate Shear Strength of a Metal-Ceramic Interface. *Acta Metall.* **1989**, *37*, 1265–1270. [[CrossRef](#)]
32. Kelly, A.; Tyson, W.R. Tensile Properties of Fibre-Reinforced Metals: Copper/Tungsten and Copper/Molybdenum. *J. Mech. Phys. Solids* **1965**, *13*, 329–350. [[CrossRef](#)]
33. Jörg, T.; Cordill, M.J.; Franz, R.; Kirchlechner, C.; Többens, D.M.; Winkler, J.; Mitterer, C. Thickness Dependence of the Electro-Mechanical Response of Sputter-Deposited Mo Thin Films on Polyimide: Insights from in-Situ Synchrotron Diffraction Tensile Tests. *Mater. Sci. Eng. A* **2017**, *697*, 17–23. [[CrossRef](#)]
34. Holmberg, K.; Matthews, A. *Coatings Tribology: Properties, Mechanisms, Techniques and Applications in Surface Engineering*, 2nd ed.; Elsevier Science: Amsterdam, The Netherlands, 2009.
35. Faurie, D.; Zighem, F.; Godard, P.; Parry, G.; Sadat, T.; Thiaudière, D.; Renault, P.-O. In Situ X-Ray Diffraction Analysis of 2D Crack Patterning in Thin Films. *Acta Mater.* **2019**, *165*, 177–182. [[CrossRef](#)]

Disclaimer/Publisher’s Note: The statements, opinions and data contained in all publications are solely those of the individual author(s) and contributor(s) and not of MDPI and/or the editor(s). MDPI and/or the editor(s) disclaim responsibility for any injury to people or property resulting from any ideas, methods, instructions or products referred to in the content.